Slip of Shuffle Screw Dislocations through Tilt Grain Boundaries in Silicon

Hao Chen[a,*], Levitas Valery[b,**], Liming Xiong[a,]

[a] *Department of Aerospace Engineering, Iowa State University, Ames, IA, 50010*
[b] *Iowa State University, Departments of Aerospace Engineering, Mechanical Engineering, and Material Science and Engineering, Ames, Iowa 50011, USA*

Abstract

In this paper, molecular dynamics (MD) simulations of the interaction between tilt grain boundaries (GBs) and a shuffle screw dislocation in silicon are performed. Results show that dislocations transmit into the neighboring grain for all GBs in silicon. For $\Sigma 3$, $\Sigma 9$ and $\Sigma 19$ GBs, when a dislocation interacts with a heptagon site, it transmits the GB directly. In contrast, when interacting with a pentagon site, it first cross slips to a plane on the heptagon site and then transmits the GB. The energy barrier is also quantified using the climbing image nudged elastic band (CINEB) method. Results show that $\Sigma 3$ GB provides a barrier for dislocation at the same level of the Peierls barrier. For both $\Sigma 9$ and $\Sigma 19$ GBs, the barrier from the heptagon sites is much larger than the pentagon sites. Since the energy barrier for crossing all the GBs at the heptagon sites is only slightly larger than the Peierls barrier, perfect screw dislocations cannot pile up against these GBs. Furthermore, the critical shear stress averaged over the whole sample for the transmission through the $\Sigma 9$ and $\Sigma 19$ GBs is almost twice on heptagon site for initially equilibrium dislocation comparing with dislocations moving at a constant velocity.

Keywords: Silicon, Shuffle Screw Dislocation, Boundaries, Dislocation Transmission, Molecular Dynamics

*haochen@iastate.edu
**vlevitas@iastate.edu
lmxiong@iastate.edu

1. Introduction

Along with other applications, polycrystalline silicon has been widely used for photovoltaic solar cells. Tremendous efforts have been made to reduce the cost and improve the energy efficiency of polycrystalline Si photovoltaic cells [1, 2] due to the vast demand for renewable solar power. The strength and ductility of polycrystalline silicon depend not only on the interaction and multiplication of dislocations, but also are determined by the interaction between dislocations and grain boundaries (GBs). However, many details of the dislocation-GB interactions in silicon are not fully understood. Experiments have shown that dislocations in silicon can either pile-up or transmit the GBs [3]. Atwater and Brown found that amorphous silicon nucleates heterogeneously at the GBs during the irradiation of polycrystalline Si thin films [4]. Using the in-situ high-voltage electron microscopy, Ballin et al.observed that dislocation with a common Burgers vector 1/2[011] transmitted from one grain to the neighboring grain [5]. Chen et al. has investigated the interaction between shuffle dislocation loops with $\Sigma 3$, $\Sigma 9$ and $\Sigma 19$ GBs [6]. They found that $\Sigma 3$ GB exhibits significantly higher resistance to dislocation transmission than $\Sigma 9$ and $\Sigma 19$ GBs. However unlike the atomistic simulations for metals[7, 8], non-periodic boundary condition along the dislocation line have been applied, which exhibits the free surface effect[6]. In order to isolate the free surface effect and the interactions between dislocations and GBs, periodic boundary condition is applied in this paper.

Also, the dislocation pile up against grain boundary was considered as a key contributors for the drastic reduction of the phase transformation pressure in materials under a large plastic shear [9, 10]. It is important to find out whether screw dislocations can pileup against GBs in Si.

This paper aims to provide a fundamental understanding on the interaction between shuffle screw dislocation and ($\Sigma 3$, $\Sigma 9$ and $\Sigma 19$) GBs. Our next paper would present results on interaction between 60^o shuffle dislocations with GBs[11].

2. The Computational Set-up

Figure 1 shows the computer models of bi-crystalline silicon, with $\Sigma 3$, $\Sigma 9$ and $\Sigma 19$ GBs in (a), (b) and (c), respectively. These are three most stable GBs among all $< 110 >$ tilt GBs and make up more than 70% of all possible GBs [6, 12, 13]. As shown in Figs. 1(a-c), grain-I in all the three models have the same crystallographic orientation with xy plane on the (111) glide plane. Periodic boundary conditions were applied in x direction with a periodicity length, $L_x \approx 4nm$. Lengths of L_x has been varied from $4nm$ to $30nm$ and results are independent of this length due to periodic boundary conditions. Along the other two directions, $L_y \approx 60nm$ and $L_z \approx 40nm$. Several layers of atoms at the two surfaces perpendicular to the y-direction are fixed. The model consists of $\sim 400,000$ atoms. Additional computer models for large samples were also constructed and it was shown that the results observed in this paper did not change with the size. To create perfect screw dislocations, e.g., with the Burgers vector $\boldsymbol{b} = 1/2[1\bar{1}0]$ [14], a constant ramped velocity v along x direction is applied on the several layers of atoms at the left boundary above and below the central glide plane and in opposite directions, as shown in Fig. 1 (a) [7, 8, 15]. In all simulations, $v = 0.001nm/ps$ and the central glide plane is put between the shuffle set to generate a perfect screw dislocation. To study the effect of dislocation velocity of the GB resistance, shear stress was applied immediately after dislocation generation near the right side of the sample. Under prescribed shear stress, dislocation in silicon reaches a stationary velocity[16] before it reaches GB. This procedure was repeated with increasing shear strain until dislocation passes through GB.

Alternatively, the static screw dislocation is inserted by applying the displacement field of a screw dislocation[15] near the GB, for example, near the heptagon defects in the first grain. The system is relaxed for $100ps$ to get the stable dislocation structure. Then shear stress is gradually increased until the dislocation transmits into the neighboring grain.

Simulations were performed at a constant temperature of $300K$ using Nosé-

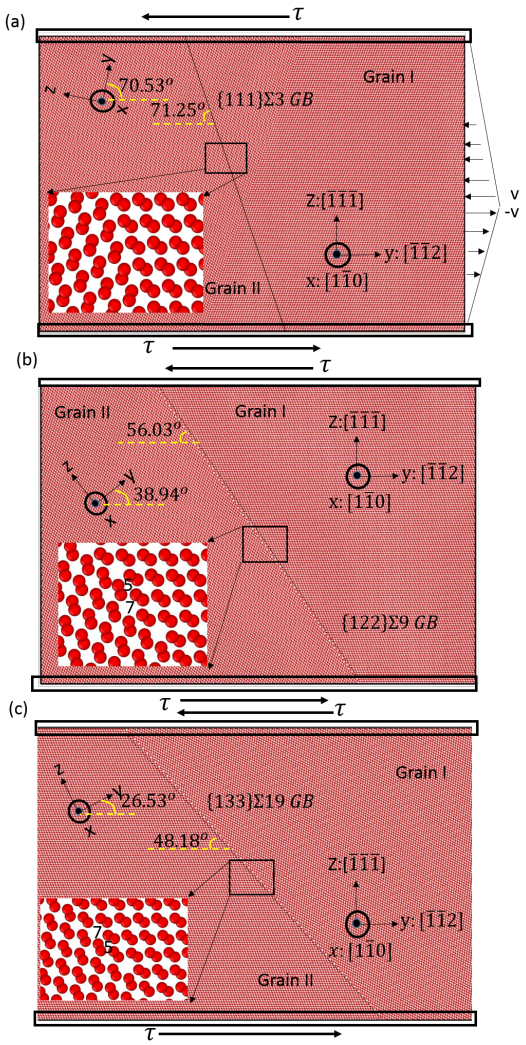

Figure 1: Computational models of bicrystalline silicon with (a) Σ3, (b) Σ9, and (c) Σ19 grain boundaries.

Hoover thermostat. Displacement corresponding to a constant shear strain (ϵ_{appl}) is applied homogeneously to the external surface of the MD cell in the $x-z$ shear plane. The atomic interactions are described by the Stillinger-Weber (SW) potential [17], which is capable to capture undissociated shuffle dislocations in silicon. The time step for all simulations is 1fs. All simulations were conducted using the Large-scale Atomic/Molecular Massively Parallel Simulator (LAMMPS) [18].

3. The Interaction between Shuffle Screw Dislocations and Grain Boundaries in Silicon

In this section, we present how perfect screw shuffle dislocations interact with different GBs. The trajectories of dislocations are tracked using the von-Mises shear strain in OVITO[19, 20, 21].

Fig. 2a shows how a shuffle screw dislocation transmits the $\Sigma 3$ GB directly. In our simulations, as long as the screw dislocation migrates in grain I, it can transmit the GB into grain II, which indicates that the $\Sigma 3$ GB also imposes no barrier for a screw dislocation motion. This is consistent with the screw dislocation behavior in bi-crystalline F.C.C. metallic materials [7]. In F.C.C. metals, the full screw dislocation dissociates into two partial dislocations. When the screw dislocations interact with twin boundaries in metal, the dissociated screw dislocations first constrict into a full screw dislocation and then transmit the GB. During the transmission procedure, the constricting process imposes the main energy barrier [7]. However, in silicon, since the screw dislocation on the shuffle set is already a full dislocation, the constricting process is not needed, consequently, $\Sigma 3$ GB acts as a low energy barrier to shuffle dislocations in silicon.

Fig. 2b presents the process of the interaction between a perfect screw dislocation with $\Sigma 19$ GB, which is composed of continuous pentagon-heptagon defects as shown in Fig. 1 [12, 6]. The perfect screw dislocation can have two different interaction sites with $\Sigma 19$ GB, i.e., the pentagon site (designated p_5 site

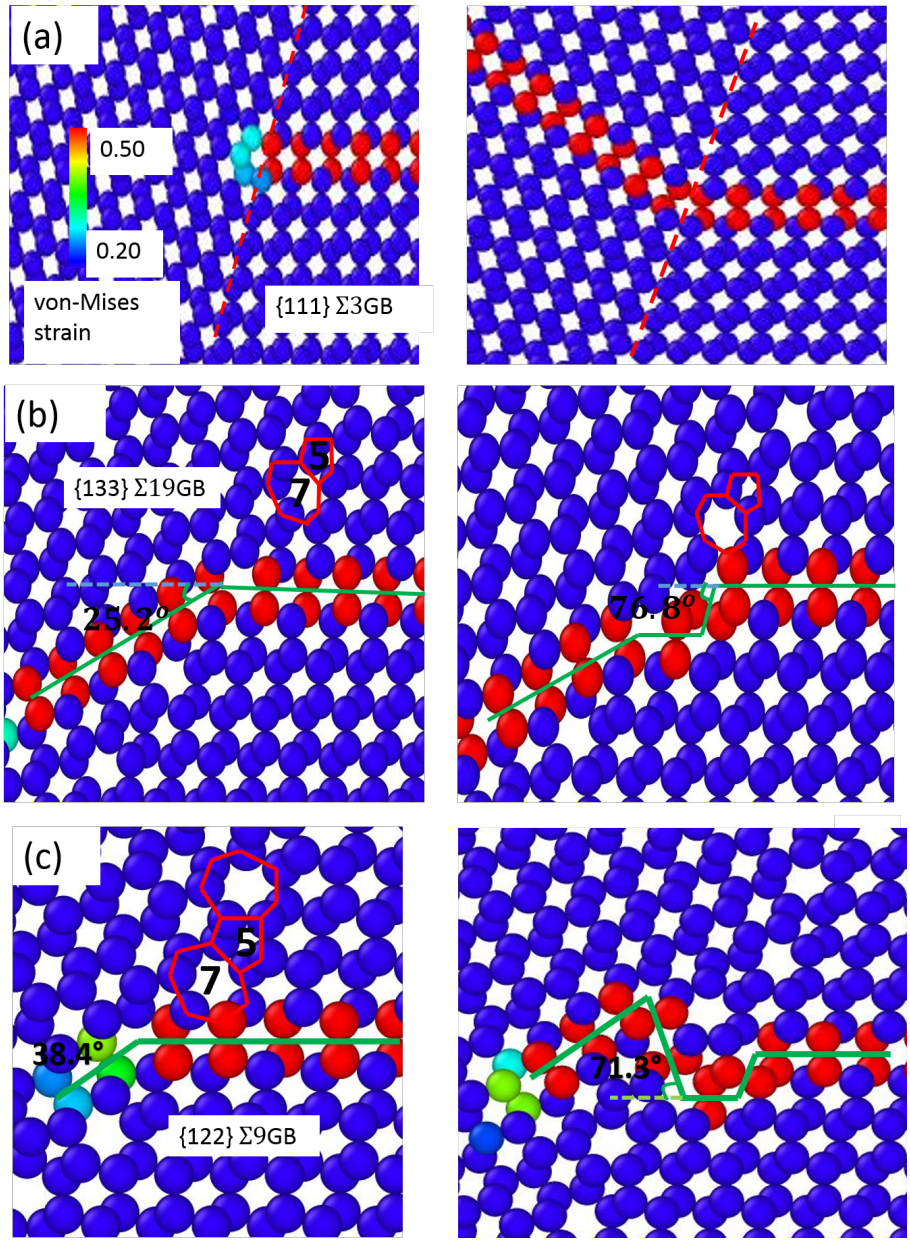

Figure 2: The atomistic process for the interactions between perfect screw dislocations and Σ3, Σ9, and Σ19 GBs. (a) The direct transmission process of a shuffle screw dislocation through the Σ3GB. (b) The transmission of a shuffle screw dislocation through the Σ19 GB. The dislocations interact with the heptogon site on the right side and the pentagon site on the left side. (c) The transmission of a shuffle screw dislocation through the Σ9 GB. The dislocation interact with the heptogon site (right) and the pentagon site (left), respectively.

below) and the heptagon site (designated p_7). When a dislocation interact with $\Sigma 19$ GB at p_7 site as shown on the left side of Fig. 2b, the dislocation switches the glide plane to the (111) plane in the neighboring grain directly, which is similar to a cross-slip behavior. However, when the dislocation interacts with the p_5 site, as shown in the right side of Fig. 2b, the dislocation first cross slips into the neighboring plane on the p_7 site in grain I and then transmits the GB. This results show that the heptagon sites act as higher energy barrier for dislocation motion than the pentagon site does. This can also be seen in the process of an interaction process between perfect screw dislocations and $\Sigma 9$ GB shown in Fig. 2c since $\Sigma 9$ is also composed of continuous pentagon-heptagons (Fig. 1). For the heptagon sites, the dislocation transmits the GB directly through a similar cross-slip behavior which is similar to that in $\Sigma 19$ GB. However, for a pentagon site, the dislocation first cross slips to the plane on the heptagon site. Then the dislocation transmits the GB to the neighboring grain to a plane with 71.3^0 inclination angle as shown on the right 2c. Thereafter, due to the large critical shear stress, it has another cross-slip in grain II to a plane with the lower critical shear stress and inclination angle [15]. This again demonstrates that the pentagon site imposes a higher energy barrier for the dislocation migration than the heptagon site does.

The climbing image nudged elastic band (CINEB) method was used to determine the energy barrier of the dislocation motion across a stress-free GB [22, 23]. In the CINEB calculations, the dislocation was created by adding the screw dislocation displacement into the sample. It can be seen that the energy barrier imposed by $\Sigma 3$ is almost the same as the Peierls barrier for dislocation motion (Fig. 3). For both $\Sigma 9$ and $\Sigma 19$ GBs, the pentagon sites generate an energy barrier of $1.9ev/nm$ while the heptagon sites produce an energy barrier around $0.6ev/nm$. This explains why the screw dislocation always transmit the GB at the heptagon sites rather than the pentagon sites. Since the energy barrier for crossing all the GBs at the heptagon sites is only slightly larger than the Peierls barrier for the dislocation motion in bulk, perfect screw dislocations cannot pile up against these GBs and cannot reduce phase transformation pres-

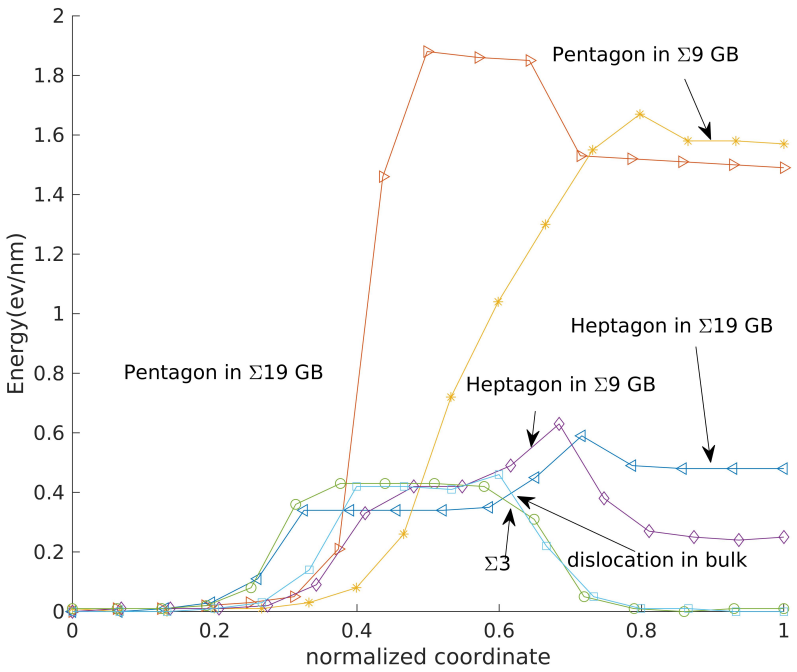

Figure 3: The energy barrier calculated by the CINEB method for Σ3, Σ9, and Σ19 GBs in silicon under stress-free state. For comparison, energy barrier for dislocation motion in bulk (without GB) is shown.

sure during plastic deformations [9, 10]. At the same time, all GBs produces 60^o dislocation pile-up, which essentially reduces the transformation pressure from Si I to Si II under shear [24, 25].

In addition, the velocity of a dislocation is also found to play an important role in the process of a dislocation-GB interaction. Here we found that the critical shear stress needed for dislocation transmission through the GB is different for moving and static dislocation. For static dislocation the critical shear stress averaged over sample is $\tau_s = 5.3$ GPa and for moving dislocation it is $\tau_d = 2.9$ GPa for Σ19 GB and $\tau_s = 5.4$ GPa and τ_d=2.9 GPa for Σ9 GB on heptagon defects. Here, the dislocation reaches a stationary speed $v = 3065m/s$ when it meets the GB under shear stress $2.9GPa$, which is far below the elastic wave

speed in silicon[26]. Interestingly, τ_d and τ_s are almost the same for $\Sigma 19$ and $\Sigma 9$ GBs, which demonstrates that the energy barrier is determined by the local structure of the GB. Thus, the energy barrier is the same for heptagon sites in $\Sigma 19$ and $\Sigma 9$ GBs and it is independent of the misorientation angle of the GBs under stress-free state [15, 7], which is similar to the screw dislocation behavior in F.C.C. metals.

4. Conclusions

In the paper, the interactions between tilt GBs and a shuffle screw dislocation in silicon are investigated using molecular dynamics. Results show that the dislocation transmits into the neighboring grain for all GBs. For $\Sigma 3$ GB, the dislocation goes through the GB directly. For $\Sigma 9$ and $\Sigma 19$ GBs, when the dislocation is on heptagon site, the dislocation transmits the GB directly as well. However, when the dislocation is on the pentagon site, it first cross slips to a plane on the heptagon site and then transmits the GB. The energy barrier was calculated using the climbing image nudged elastic band method. Results show that $\Sigma 3$ GB generates the barrier at the level of the Peierls barrier. For both $\Sigma 9$ and $\Sigma 19$ GBs, the barrier for dislocation transmission of heptagon sites is $0.6ev/nm$, while it is $1.9ev/nm$ for pentagon defects. Furthermore, we found that the critical shear stress for the transmission is lowered from $5.3GPa$ to $2.9GPa$ for moving dislocation versus the static dislocation. Since energy barrier for crossing the $\Sigma 3$ is equal to the Peierls barrier for dislocation motion in bulk, and for $\Sigma 9$ and $\Sigma 19$ GBs at the heptagon defects it is only slightly larger than the Peierls barrier, perfect screw dislocations cannot pile up against these GBs and cannot reduce phase transformation pressure during plastic deformations [9, 10].

5. Acknowledgements

We acknowledge the support of NSF (Grant No.CMMI-1536925) and the Extreme Science and Engineering Discovery Environment (XSEDE allocations TG

MSS170003). VIL also acknowledges supports of ARO (W911NF-17-1-0225), ONR (N00014-16-1-2079) and the ISU (Vance Coffman Faculty Chair Professorship).

References

[1] A. Shah, P. Torres, R. Tscharner, N. Wyrsch, H. Keppner, Photovoltaic technology: the case for thin-film solar cells, science 285 (5428) (1999) 692–698.

[2] M. Tanaka, Recent progress in crystalline silicon solar cells, IEICE Electronics Express 10 (16) (2013) 20132006–20132006.

[3] M. Martinez-Hernandez, H. Kirchner, A. Korner, A. George, J. Michel, Dislocations at grain boundaries in deformed silicon, Philosophical Magazine A 56 (5) (1987) 641–658.

[4] H. A. Atwater, W. L. Brown, Grain boundary mediated amorphization in silicon during ion irradiation, Applied Physics Letters 56 (1) (1990) 30–32.

[5] X. Baillin, J. Pelissier, J. Bacmann, A. Jacques, A. George, Dislocation transmission through= 9 symmetrical tilt boundaries in silicon and germanium: I. in situ observations by synchrotron x-ray topography and high-voltage electron microscopy, Philosophical Magazine A 55 (2) (1987) 143–164.

[6] X. Chen, L. Xiong, A. Chernatynskiy, Y. Chen, A molecular dynamics study of tilt grain boundary resistance to slip and heat transfer in nanocrystalline silicon, Journal of Applied Physics 116 (24) (2014) 244309.

[7] Z.-H. Jin, P. Gumbsch, E. Ma, K. Albe, K. Lu, H. Hahn, H. Gleiter, The interaction mechanism of screw dislocations with coherent twin boundaries in different face-centred cubic metals, Scripta Materialia 54 (6) (2006) 1163–1168.

[8] Z.-H. Jin, P. Gumbsch, K. Albe, E. Ma, K. Lu, H. Gleiter, H. Hahn, Interactions between non-screw lattice dislocations and coherent twin boundaries in face-centered cubic metals, Acta Materialia 56 (5) (2008) 1126–1135.

[9] V. I. Levitas, M. Javanbakht, Phase transformations in nanograin materials under high pressure and plastic shear: nanoscale mechanisms, Nanoscale 6 (1) (2014) 162–166.

[10] M. Javanbakht, V. I. Levitas, Phase field simulations of plastic strain-induced phase transformations under high pressure and large shear, Physical Review B 94 (21) (2016) 214104.

[11] L. X. Hao Chen, Valery Levitas, Amorphous phase in silicon induced by 60^o dislocations pile-up against different grain boundaries, to be published.

[12] M. Kohyama, R. Yamamoto, M. Doyama, Structures and energies of symmetrical¡ 011¿ tilt grain boundaries in silicon, physica status solidi (b) 137 (1) (1986) 11–20.

[13] S. Ratanaphan, Y. Yoon, G. S. Rohrer, The five parameter grain boundary character distribution of polycrystalline silicon, Journal of materials science 49 (14) (2014) 4938–4945.

[14] W. Cai, V. V. Bulatov, J. Chang, J. Li, S. Yip, Dislocation core effects on mobility, Dislocations in solids 12 (2004) 1–80.

[15] D. Hull, D. J. Bacon, Introduction to dislocations, Butterworth-Heinemann, 2001.

[16] C.-x. Li, Q.-y. Meng, G. Li, L.-j. Yang, Atomistic simulation of the 60 dislocation mobility in silicon crystal, Superlattices and Microstructures 40 (2) (2006) 113–118.

[17] L. Pizzagalli, J. Godet, J. Guénolé, S. Brochard, E. Holmstrom, K. Nordlund, T. Albaret, A new parametrization of the stillinger–weber potential

for an improved description of defects and plasticity of silicon, Journal of Physics: Condensed Matter 25 (5) (2013) 055801.

[18] S. Plimpton, Fast parallel algorithms for short-range molecular dynamics, Journal of computational physics 117 (1) (1995) 1–19.

[19] A. Stukowski, Visualization and analysis of atomistic simulation data with ovito–the open visualization tool, Modelling and Simulation in Materials Science and Engineering 18 (1) (2009) 015012.

[20] M. L. Falk, J. S. Langer, Dynamics of viscoplastic deformation in amorphous solids, Physical Review E 57 (6) (1998) 7192.

[21] F. Shimizu, S. Ogata, J. Li, Theory of shear banding in metallic glasses and molecular dynamics calculations, Materials transactions 48 (11) (2007) 2923–2927.

[22] G. Henkelman, H. Jónsson, Improved tangent estimate in the nudged elastic band method for finding minimum energy paths and saddle points, The Journal of chemical physics 113 (22) (2000) 9978–9985.

[23] G. Henkelman, B. P. Uberuaga, H. Jónsson, A climbing image nudged elastic band method for finding saddle points and minimum energy paths, The Journal of chemical physics 113 (22) (2000) 9901–9904.

[24] V. I. Levitas, Phase transformations under high pressure and large plastic deformations: Multiscale theory and interpretation of experiments, in: Proceedings of the International Conference on Martensitic Transformations: Chicago, Springer, 2018, pp. 3–10.

[25] V. I. Levitas, H. Chen, L. Xiong, Phase transitions and their interaction with dislocations in silicon, in: Proceedings of the International Conference on Martensitic Transformations: Chicago, Springer, 2018, pp. 83–87.

[26] E. Hahn, S. Zhao, E. Bringa, M. Meyers, Supersonic dislocation bursts in silicon, Scientific reports 6 (2016) 26977.